Suresh Goyal
Member of Technical Staff,
Wireless Research Laboratory,
Lucent Technologies Bell Laboratories,
600 Mountain Avenue, Rm. 1B-212,
Murray Hill, NJ 07974

Ronald G. Larson
Professor, Department of
Chemical Engineering,
University of Michigan,
Ann Arbor, MI 53214

Charles J. Aloisio
Distinguished Member of Technical Staff,
Lucent Technologies Bell Laboratories,
2000 Northeast Expy, Rm. 2H37,
Norcross, GA 30071

Quantitative Prediction of Impact Forces in Elastomers

We measure the impact forces and deflections resulting from drop tests of a mass with a flat impact surface onto flat pads of various elastomeric materials, and show that the forces can be predicted quantitatively with no adjustable parameters by using a theory whose only inputs are the linear viscoelastic characteristics of the material, measured in small-amplitude oscillatory deformations. The theory, which models the elastomer as a nonlinear neo-Hookean material, is accurate for several elastomeric solids including polyurethanes, polynorbornene, and poly-vinyl-chlorides (PVCs), over a wide range of impact velocities, masses, temperatures and pad thicknesses. Some steps are taken to extend the model to surfaces which are not flat. The application in mind is the rational design of elastomeric components in impact-tolerant portable electronic equipment.

1 Introduction

It is highly desirable that portable electronic products, like notebook computers, cellular phones, etc., be able to withstand accidental drops and bangs against hard, unyielding, surfaces (Goyal et al., 1998c). In optimizing the impact-tolerance of a portable product, its designer faces two challenges:

(1) Predicting impact-induced loads, and,
(2) Devising strategies for controlling impact loads within stringent constraints that require small size, light weight, low cost and mass-manufacturability.

Goyal et al. (1997, 1998a, 1998b) have shown that the use of highly dissipative viscoelastic materials in shock-absorbing components like suspensions, grommets, gaskets, and plastic housings is effective in improving the drop-tolerance of portable products.

This paper addresses the issue of predicting forces that would occur in impacts mediated through elastomers. The aim is to facilitate rational design of shock and vibration absorbing viscoelastic elements in equipment. Accurate modeling of impacts forces in polymers is challenging because it involves both geometric complexity and material complexity. That is, impacts usually involve two or three dimensional shape changes that are time-dependent and so involve the time-dependent or viscoelastic properties of the materials involved in the impact. Complex geometric effects can be accounted for by finite element analysis; however, the material properties assumed in such analyses are usually those of a simple Hookean elastic solid described by a single modulus value, or more elaborate empirical models that involve parameters that do not relate directly to measurable material properties (e.g., Burnett, 1987). This approach can be successful for hard crystalline or glassy polymers such as those used in car bumpers, side panels, etc., where stresses are large and deformations prior to yield are small. However, for soft elastomeric materials, such as those used as shock absorbers in portable electronic devices, deflections are large (strains can be greater than 50%), and the response of the material is controlled by a whole spectrum of relaxation processes that dissipate energy over a large range of time scales. For such materials, a Hookean solid is an unacceptably poor model, and the actual spectrum of relaxation processes of the material must be included in the model, if it is to be even qualitatively accurate. Hence, modeling impacts involving elastomers requires an approach that differs considerably from that of traditional impact modeling methods, which focus primarily on geometric complexity rather than material complexity. Here, however, we shall develop an approach that emphasizes, first and foremost, accurate modeling of the viscoelastic properties of the material. An added advantage of this approach is that it inherently also captures the temperature-dependent behaviour of the elastomer—which is considerable. In the future, we envision that our material model will be combined with accurate finite-element modeling of geometric complexity.

In an earlier paper (Larson et al., 1996), we showed that a simple constitutive equation for a neo-Hookean rubber could be used to give accurate predictions of impact forces in ideal drop tests of flat objects on thick flat pads of a polyurethane elastomer (called 'Sorbothane') as measured with a commercial drop tester. In essence, we demonstrated the possibility of using simple and easily obtained linear viscoelastic properties of an elastomer to predict impact forces in ideal impacts, shown in Fig. 1(*a*). In this paper, we carry that work forward toward realizing the vision of optimal design of elastomeric parts using analytical methods.

First we show that our predictive model for impact forces is accurate for solid elastomeric materials in general, by studying several other materials. We chose commercially available materials for our study that are recommended for shock-protection purposes because of their remarkably high damping properties, and whose compositions vary from that of Sorbothane—a polyurethane. We show that agreement similar to that found for Sorbothane is obtained for:

(1) 'Wingfoot XL', a material based on the amorphous polymer polynorbornene, manufactured by Goodyear Shoe Products, Hudson, NH.
(2) E.A.R. C-1002, a PVC material, made by E.A.R. Specialty Composites, Indianapolis, IN.
(3) 'Impactek,' a material marketed by Frelonic Corporation, Salem, MA.

Then we demonstrate that the predictive model can give qualitatively correct results even for impacts involving very thin pads of these elastomers, as thin as those that are likely to be used in applications. In such thin pads, deformations and the resulting impact forces become very high. Hence, the possibility

Contributed by the Materials Division for publication in the JOURNAL OF ENGINEERING MATERIALS AND TECHNOLOGY. Manuscript received by the Materials Division August 20, 1998; revised manuscript received December 18, 1998. Associate Technical Editor: G. Ravichandran.

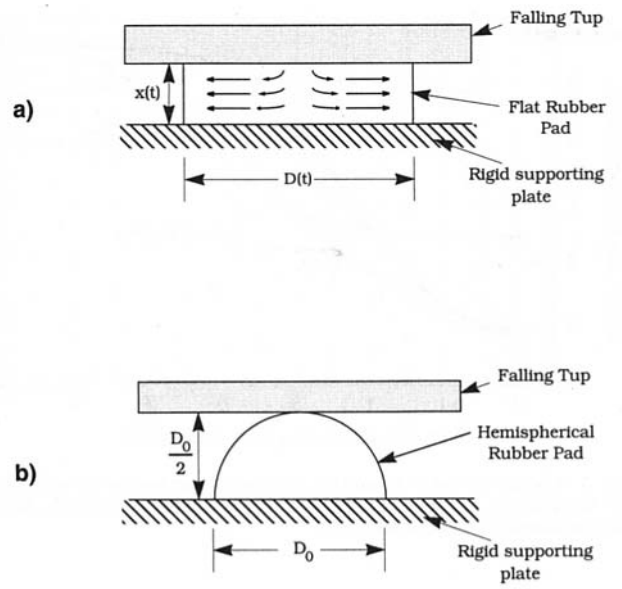

Fig. 1 Schematic of impacts mediated through elastomeric pads. (*a*) Ideal impact, flat pad; (*b*) nonideal impact, hemispherical pad.

of nonuniform deformation increases, due to possible adhesion between the impacting surface and the elastomer pad, and due to the short time scales of the impact process, which may be insufficient for the damping out of 'viscoelastic shock waves' on the time scale of the impact. We show that although the latter factor may play a role in impacts on thin pads, the important parameters of the impact, namely its peak force, its duration, and the maximum deflection of the elastomer pad (Goyal et al., 1997), can still accurately be predicted by the simple model, without addition of any arbitrary fitting parameters.

We also develop a semi-empirical method that allows the theory for flat pads to be applied in an approximate way to nonideal impacts involving a hemi-spherical surface impacting a flat one, as might occur when the corner of a laptop computer or cellphone impacts a hard surface.

The layout of the paper is as follows. In the next section, we describe the linear viscoelastic properties of Wingfoot XL and Sorbothane 70, and very briefly those of E.A.R. C-1002 and Impactek. Then, the experimental drop-test results are presented, including results at different temperatures, and results obtained for thin pads; these are compared to the behavior predicted using the neo-Hookean model with the viscoelastic properties measured for the above materials. We then consider nonideal impacts. Finally sample cushioning efficiency curves are calculated for Wingfoot XL, and the results summarized.

2 Experimental Results

Two basic kinds of experiments were performed on each material selected for our study: (a) measurement of the linear viscoelastic spectrum (also known as the "master curve," or the "reduced frequency nomogram"), and, (b) measurement of forces and deflections in drop tests involving pads of the material.

2.1 Selected Dissipative Elastomers—Compositions. The four elastomeric solids whose results we present in this paper represent different methods of engineering polymers to have high damping at room temperature and be effective for shock-protection. The properties of Sorbothane were discussed at length in our previous paper (Larson et al., 1996). The material we will consider in greatest detail in this paper is Wingfoot XL. The other materials, E.A.R. C-1002 and Impactek, are considered briefly but will be examined further, along with their foamed versions, in a forthcoming publication.

As discussed in Larson et al. (1996), high energy dissipation during impact (or shock-absorption) at a given temperature occurs in elastomers that are in their "viscoelastic transition zones" between rubbery and glassy behavior at that temperature, for frequencies characteristic of typical impacts, around $10^2 - 10^4\ s^{-1}$. Equivalently, a high rate of viscous dissipation can most readily be achieved in a material whose glass transition temperature T_g is a few tens of degrees Celsius below the temperature at which impact occurs.[1] The amount of viscous damping is controlled by the extent of the transition zone. The sharper the transition zone, the higher the viscous dissipation during impact.[2] However, a sharp transition zone also implies that mechanical properties of the polymer are very sensitive to temperature (and frequency) changes. So, good impact-absorbing performance over a wider effective temperature range frequently comes at the expense of lower dissipativeness.

There are several methods of engineering polymers to have the above properties. In the case of Sorbothane a single-phase material is found with the appropriate T_g, and the crosslink density is kept low to yield a transition zone in the $10^2 - 10^4\ s^{-1}$ frequency window at room temperature. The $T_g = -59.5°C$ for Sorbothane 70, determined using the 'WLF fit' method to be described in the next section, is acceptable but perhaps a bit too low for an ideal impact response at room temperature. However, the strategy followed in the formulation of Wingfoot XL is quite different, namely addition of a plasticizer[3] to a high T_g material to soften it to the desired extent.

The composition of Wingfoot XL (Pilkington et al., 1985), by weight, is roughly 10 parts polynorbornene,[4] 14 parts paraffinic oils, and 4 parts resin (Pilkington, 1995). The resin is incompatible with polynorbornene and together they form an eutectic mixture—an example being glycol and water. The resin essentially acts like a filler (Rosen, 1993), acting to modify the modulus. Polynorbornene is by itself a glassy polymer ($T_g = 43°C$) but in powdery form it has tremendous affinity for paraffinic oils and can absorb and retain a large amount of them due to its cage-like molecular structure. The paraffinic oils act as plasticizers to lower the glass transition temperature of polynorbornene. It is this interaction between the paraffinic solvent and polynorbornene that gives Wingfoot XL a highly dissipative character at room temperature.

E.A.R. C-1002 is a plasticized PVC (E.A.R., 1996; Seville, 1998). The plasticizer is a medium-to-high molecular weight oil with a low migration rate. We do not know the composition of Impactek.

As a final remark, we note that in addition to the two strategies mentioned above for designing impact-protecting elastomers, namely, finding a single-phase material with a suitable T_g, and using a plasticizer to tune T_g to a suitable value, there are at least two other strategies for optimizing the impact characteristics of a material. One is to either use blends of two different polymers, or use "block copolymers" (Ferry, 1980) with two or more blocks of chemically different composition, to tune the dissipative characteristics of the elastomer for optimum impact protection. This third strategy has been followed in the design of a block copolymer with polystyrene and modified polyisoprene blocks copolymer known as "VS polymer," manufactured by Kuraray of Japan and marketed as an impact-protecting material. A fourth strategy is to foam a polymer, thereby reducing its modulus. Both of these latter two strategies will be discussed in a subsequent paper.

[1] The other significant factor in determining the usefulness of an elastomer in shock-protection applications is its dynamic modulus.

[2] The slope of the elastic modulus in the master curve for the material is related to tan δ, the loss factor (Ferry, 1980).

[3] A plasticizer is an additive to a polymer that reduces its T_g (Rosen, 1993). Commonly used plasticizers are oils of various densities.

[4] Polynorbornene is distributed in the U.S. by Zeon Chemicals, Inc., Rolling Meadows, IL.

Table 1 Viscoelastic shift factors for reference T = 20°C

	$\log_{10} a_T$		
Temperature °C	Wingfoot XL	E.A.R. C-1002	Impactek
−80	—	14.3	11.18
−70	—	13.5	10.98
−60	—	13	10.58
−50	8.96	12	10.18
−40	8.56	10.2	9.68
−30	8.16	8	9.08
−20	6.96	6	7.37
−9	5.26	4	5.47
0	3.16	2.4	3.25
10	1.46	0.5	1.5
20	0	0	0
30	−1.11	−1	−1.4
40	−1.94	−1.8	−2.61
50	−2.91	−3.4	−3.42
61	—	—	−4.22
70	—	—	−4.62
80	—	—	−5.02

2.2 Viscoelastic Measurements. Viscoelastic properties of Wingfoot XL and the other elastomers used in our study were characterized through small-amplitude oscillatory tests using the Rheometrics Solids Analyzer (RSA) in tension-tension mode, as described in our previous paper (Larson et al., 1996). The Wingfoot XL sample was 10.4 mm long, 3.86 mm wide, and 1.96 mm thick. The applied strain amplitude was 0.1%. At the lowest temperature of −50°C, a static tensile force equivalent to 100 gms was applied and at the highest temperature, 50°C, this was reduced to zero.

At each of the temperatures in Table 1, the tensile storage modulus E' and the tensile loss modulus E'' were measured at frequencies ω ranging from 0.1−100 rad/s. Because of the equivalent effect of frequency and temperature (Ferry, 1980), in the absence of any structural or chemical changes during the test, the moduli at each individual temperature can be shifted along the log frequency axis to form a master curve at the reference temperature of 20°C. The shift factors a_T for Wingfoot XL at each temperature are tabulated in Table 1; and the master curve appears in Fig. 2.

The shear storage and loss moduli, G' and G'', are related to the corresponding tensile moduli by

$$G' = \frac{E'}{2(1+\nu)}; \quad G'' = \frac{E''}{2(1+\nu)} \tag{1}$$

In the low-frequency, low-modulus, rubbery zone, Poisson's ratio is time-independent and has a value of $\nu \approx 0.5$, and Eq. (1) reduces to $G' = E'/3$, and $G'' = E''/3$. These relationships are used for all of the data in Fig. 2. Although these relationships are not exact in the high-frequency, high-modulus, glassy zone, data in this region are not particularly important to the impact properties of the material, at least at or above room temperature.

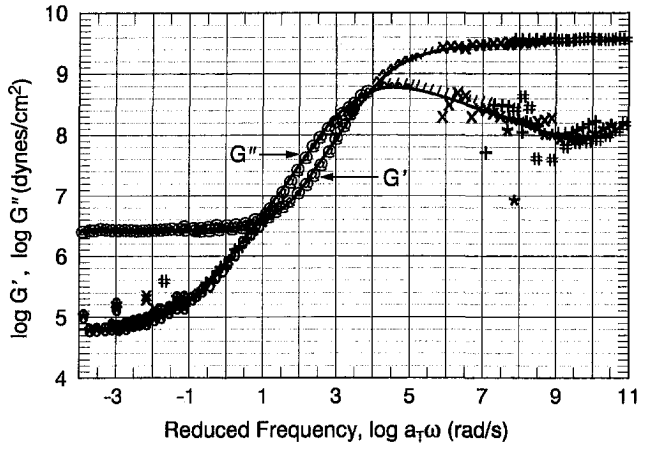

Fig. 2 Master Curve of G' and G'' versus reduced frequency log ($a_T\omega$) for Wingfoot XL, at a reference temperature of 20°C. It is the superposed curve produced by shifting "dynamic modulus isotherms," obtained at each temperature listed in Table 1, along the reduced frequency axis by an amount log a_T (also given in Table 1).

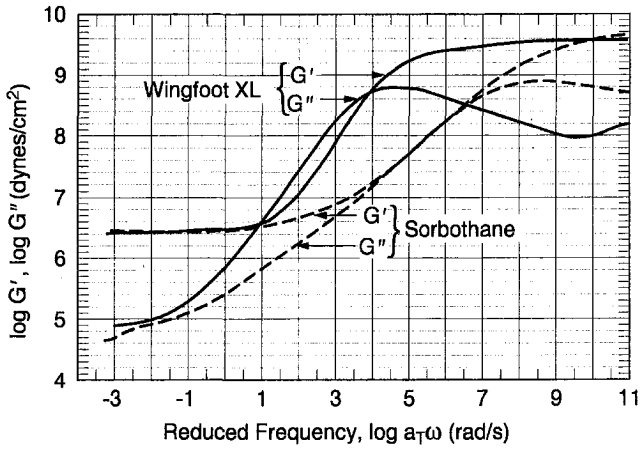

Fig. 3 Master Curves of G' and G'' versus reduced frequency log ($a_T\omega$) for Wingfoot XL and for Sorbothane 70 (from Larson et al., 1996), both at a reference temperature of 20°C.

Figure 3 compares the Wingfoot XL master curves with the corresponding master curves for Sorbothane 70. Wingfoot XL has a higher modulus than Sorbothane in the frequency window important for impact absorption; $G' \sim 10^6 - 10^8$ Pa for Wingfoot XL compared to $G' \sim 10^6$ Pa for Sorbothane in $a_T\omega \sim 10^2 - 10^4$ rad/s.[5] Wingfoot XL is also more dissipative than Sorbothane; that is, for Wingfoot XL, $\tan\delta \equiv G''/G' > 1$ over the whole impact-frequency window, with a maximum $\tan\delta = 2.5$, while for Sorbothane, $\tan\delta \leq 1$. As we shall see, these properties of Wingfoot XL make it better suited than Sorbothane as an impact absorber at room temperature.[6]

The shift factors log a_T obtained during the construction of the master curve for a given material can be plotted versus temperature, as shown in Fig. 4 for Wingfoot XL and Sorbo-

[5] For the available cushioning space, and masses, of portable devices like cellular phones and notebook computers, a storage modulus of 10^6–10^7 Pa seems optimal to protect against drops from 1.5 m.

[6] Chen and Lakes (1990) argue that tan δ around 1–2 near room temperature for a material make it an ideal impact-absorber.

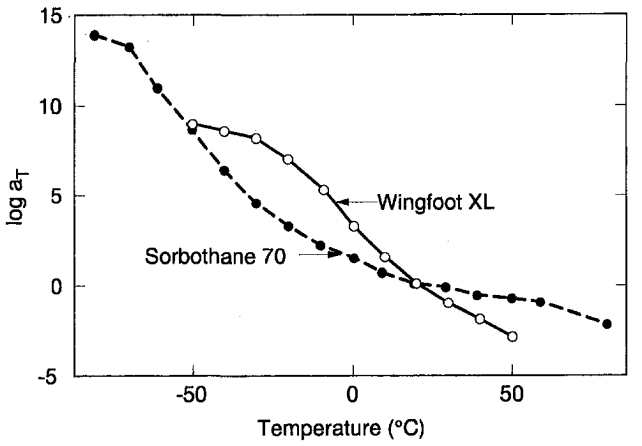

Fig. 4 Plot of the temperature dependences of the shift factors used to obtain the master curves of Figs. 2 and 3, for Wingfoot XL and Sorbothane 70.

thane 70. For polymers that form glassy solids when cooled, such as the elastomers considered here, it has been found empirically that the curve of log a_T versus temperature T can be fit by a simple expression, known as the "WLF equation," which is (Ferry, 1980)

$$\log a_T = -\frac{c_1^0(T - T_0)}{c_2^0 + T - T_0} \tag{2}$$

where T_0 is a reference temperature arbitrarily chosen from within the experimental data range, and c_1^0 (inversely proportional to the free volume, i.e., the free space between molecules) and c_2^0 (proportional to the ratio of the free volume, to the thermal expansion coefficient of that free volume) are parameters used for fitting the curve at the reference temperature. Furthermore, c_1^0 and c_2^0 can be related to constants at any other temperature, say the glass transition temperature T_g, as (Ferry, 1980)

$$c_1^0 = \frac{c_1^g c_2^g}{c_2^g + T_0 - T_g}, \quad c_2^0 = c_2^g + T_0 - T_g \tag{3}$$

For many viscoelastic polymers, it has been found that,

$$c_1^g \approx 17.44 \tag{4}$$

Having determined c_1^0 and c_2^0 from the shift factors used in the construction of the master curve for a material, and using Eqs. (3)–(4), T_g for the material can now be evaluated.[7]

Using the above described WLF fit to the data of Fig. 4, a glass transition temperature of −3.5°C was determined for Wingfoot XL. Its thermal expansion coefficient for the free volume was estimated to be 2.673×10^{-4} deg C^{-1}, and c_2^g = 93.15. Observe in Fig. 4 that near room temperature, the slope of the plot of the shift factor versus temperature is steeper for Wingfoot XL than that for Sorbothane 70, implying that the former is more temperature sensitive. Thus, the ideal impact-absorbing properties of Wingfoot XL erode quickly with temperature. On the other hand, the lower T_g = −59.5°C of Sorbothane 70, coupled with the lower temperature sensitivity of its shift factor, make Sorbothane 70 a better impact-absorber than Wingfoot XL at low temperatures.

Comparison of Wingfoot XL with Sorbothane 70 highlights the conflict between two desirable rheological properties of shock-absorbing elastomers, namely, tan δ should be greater than unity near room temperature and yet not be too temperature sensitive. Normally, tan $\delta > 1$ near its peak value, which is in the transition region for materials (like Wingfoot XL) that show a steep change in their dynamic moduli from glassy to rubbery behavior. However, rapid changes in moduli in the transition zone also implies that the viscoelastic properties of the material are very sensitive to changes in room temperature. Hence, as mentioned in Section 2.1, optimal design of a viscoelastic elastomer for shock-protection will generally involve a trade-off between its dissipative properties and its temperature sensitivity.

Table 1 also tabulates the shift factors used in the construction of the master curves for E.A.R. C-1002 and Impactek. Using a WLF fit to this data, for E.A.R. C-1002 a T_g = −5.2°C was determined; its thermal expansion coefficient for the free volume was estimated to be 2.068×10^{-4} deg C^{-1}, and c_2^g = 120.40. Similarly, for Impactek a T_g = 15.2°C was determined; its thermal expansion coefficient for the free volume was estimated to be 2.224×10^{-4} deg C^{-1}, and c_2^g = 111.96.

2.3 Discrete Fits to Dynamic Moduli. The viscoelastic response, or the evolution of stress, in the elastomer during impact can be modeled as arising from a spectrum of exponentially decaying relaxation phenomenon (p. 88, Larson, 1988; p. 156, Macosko, 1994). Hence the frequency dependent storage and loss moduli $G'(\omega)$ and $G''(\omega)$ can, in general, be fitted to expressions involving spectrum of relaxation times τ_i and strengths G_i:

$$G'(\omega) = \sum_i \frac{G_i \omega^2 \tau_i^2}{1 + \omega^2 \tau_i^2}; \quad G''(\omega) = \sum_i \frac{G_i \omega \tau_i}{1 + \omega^2 \tau_i^2} \tag{5}$$

For purposes of impact modelling (to be described in Section 3.1) the G' and G'' curves need only be fit out to the highest frequencies that influence the impact forces; typically, fits out to a frequency of around 10^4 s^{-1} are adequate (as shown earlier in Larson et al., 1996). Note that the highest frequency for which a fit is obtainable is set by the reciprocal of the shortest relaxation time τ_i in the assumed spectrum. If the fit is extended to include frequencies higher than 10^5 s^{-1}, relaxation times that are shorter than necessary are brought into the relaxation spectrum, and this greatly increases the computation required for simulation of the drop tests. (The time step for explicit integration in our simulation has to be smaller than the smallest relaxation time in the spectrum to preserve numerical stability.)

Hence, it is desirable to exclude from the set of relaxation times those values that are too short to influence the impact forces. Such very fast modes are almost completely relaxed out on the time scale of the impact—typically a few milliseconds (ms)—and contribute only a small viscous-like dissipative stress, which can be characterized by a viscosity η.[8] The validity of using a viscous term to represent high-frequency relaxation modes is a well established principle in rheology.

Therefore, we choose a set of 12–16 well spaced relaxation times (the τ_i's) spanning the time range of interest, and adjust values of the corresponding G_i's to obtain a fit of Eq. (5) to G' and G'' for each material. We regularly checked the validity of this approach by doing calculations with more modes and a correspondingly smaller viscosity, and in each case used a sufficient number of high-frequency modes to obtain results that do not change if even smaller time constants are included (see, for example, Fig. 8).

In the simulations to be described in Section 3.1, the viscosity η is shifted along with the relaxation spectrum to account for changes in temperature; that is, η and the τ_i's are multiplied by the same temperature-dependent shift factor a_T. Since changes in temperature shift the G' and G'' curves along the frequency axis, the number of "relaxation modes" (pairs of G_i and τ_i values) that must be included in the spectrum depends on the test temperature. Also, for fast impacts produced by drops onto thin pads, more modes must be included to obtain accurate predictions of the high-frequency response.

Table 2 gives the "best-fit" values of the G_i's corresponding to a set of specified τ_i's for Wingfoot XL, E.A.R. C-1002 and Impactek. For Wingfoot XL, several different viscosities are presented in Table 2. Each viscosity corresponds to the cut-off relaxation time listed in the same row of Table 2. For instance, η = 5000 Poise represents the viscosity due to all the relaxation modes that are faster than 0.001 s and η = 2 Poise represents the viscosity due to all the relaxation modes that are faster than 0.000001 s. Note that as higher and higher modes are included, the viscosity term gets smaller and smaller.

Figure 5 shows the fits to G' and G'' obtained by the 13-mode spectrum (with η = 5000 Poise) and by the 16-mode spectrum (with η = 2 Poise). For high-temperature drop tests at T = 40°C, the 13-mode spectrum is adequate, while at low temperatures, T = 5°C, the 16-mode spectrum is used. The accuracy of these representations, as mentioned earlier, was

[7] Note that the determination of T_g, using either the WLF fit method or more exact methods like "differential specific calorimetry," is not necessary for the predictive scheme presented in our paper. However, it may be useful for matching materials to applications.

[8] Analogously, modes much slower than the frequencies of interest could be lumped into a purely elastic term, with an infinite relaxation time. Inclusion of slowly relaxing modes, however, does not force a reduction in integration time step size and so is not numerically expensive.

Table 2 Viscoelastic constants at 20°C

		Wingfoot XL		E.A.R. C-1002		Impactek	
i	$\tau_i(s)$	G_i (Pa)	η (Poise)	G_i (Pa)	η (Poise)	G_i (Pa)	η (Poise)
1	10000	0.25e+06		1.5e+06		0.80e06	
2	1000	0.004e+06		0.015e06		0.008e06	
3	100	0.004e+06		0.05e06		0.12e06	
4	30	0.004e+06		0.015e06		0.08e06	
5	10	0.010e+06		0.10e06		0.14e06	
6	3	0.015e+06		0.15e06		0.20e06	
7	1	0.040e+06		0.2e06		0.25e06	
8	0.3	0.050e+06		0.4e06		0.55e06	
9	0.1	0.06e+06		0.5e06		0.90e06	
10	0.03	0.20e+06		0.7e06		0.90e06	
11	0.01	0.6e+06		1.2e06		1.05e06	
12	0.003	1.5e+06		2.0e06		2.0e06	
13	0.001	1.1e+07	5000	0.8e07		3.0e07	
14	0.0001	8.0e+07	500	2.0e07		9.9e07	
15	0.00001	1.0e+08	20	0.7e08	50	2.0e08	100
16	0.000001	5.0e+07	2				

checked by repeating some simulations using a higher number of modes. For E.A.R. C-1002 and Impactek, a 15-mode spectrum (cutoff relaxation time $\tau_i = 0.00001$ s) proved adequate for the room temperature impact simulations presented in this paper.

2.4 Drop Tests. Drop-test data for the rubber pads were collected using Dynatup impact testing machine Model 8250, shown schematically in Fig. 6. The main element of the machine is a variable mass, called the crosshead, that can be dropped from a given height onto the rubber pad being tested. High impact velocities can be obtained by propelling the crosshead with springs. The crosshead is guided on frictionless vertical rails to control its orientation. The impact force is measured through a load cell mounted on the element of the crosshead that first makes contact, which is the tup. Different inserts can be screwed to the tup to change contact geometry. The specimen temperature can be controlled in an environmental chamber.

An automated data acquisition system collects and analyzes the data. The tup inserts were 13 mm thick, and the load cell length about 125 mm so it could accurately measure the impact loads in the elastomeric pads—typically of several miliseconds duration. Depending on impact duration, an anti-aliasing filter of 12–50 KHz was used during data collection. Besides the initial impact velocity—measured independently through an optical sensor—all other quantities like accelerations, pad deflection, etc., are calculated from the force measurement by integration.

We used cylindrical tup inserts made of Aluminum 7075 with flat contacting areas varying in diameter from 38.1 to 50.8 mm, elastomer pads ranging from 25.4 to 38.1 mm in diameter; and thicknesses of 3.05 to 25.4 mm. The diameter of the tup was kept much larger than the pad diameter in all drop-tests to ensure uniform deformation of the flat pad. The crosshead mass was around 1.81 kg at room temperature and around 2.26 kg at lower or higher temperatures. The flat supporting plate was made of Stainless Steel 350 with a blanchered ground finish to ensure flatness.

Impact data were collected at room temperature (which varied from run to run from 20°C to 26°C), at 5°C, and at 40°C. The simulations were carried out using the viscoelastic spectrum shifted to the temperature at which the run was made.

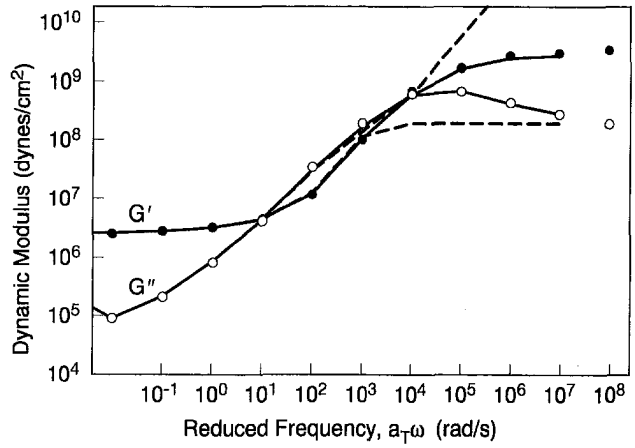

Fig. 5 Fit of G' and G'' using the 16-mode spectrum in Table 2, plus a viscous term with a viscosity of 2 Poise (solid lines) and the fit of the 13-mode spectrum with a viscosity of 5000 Poise (dotted line), compared to the linear viscoelastic data for Wingfoot XL, shifted to 20°C

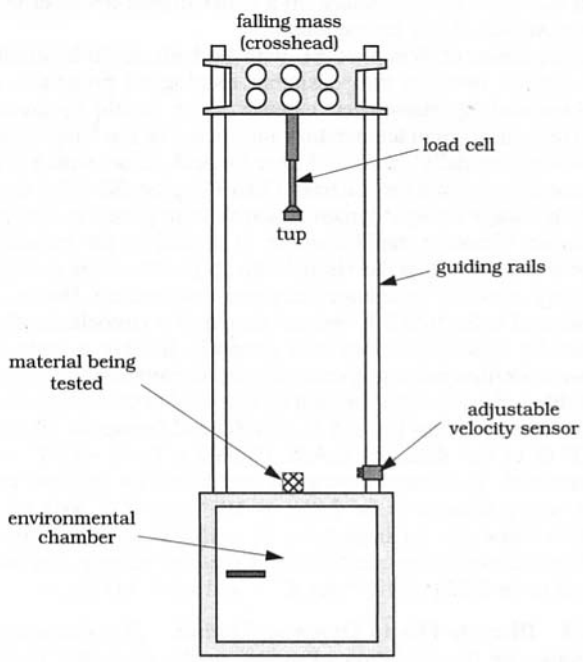

Fig. 6 Schematic of Dynatup impact testing machine Model 8250 used to test the impact response of rubber pads. The machine allows a known mass (the crosshead) to be dropped from a given height onto the material being tested. Drop orientation is controlled through frictionless guiding rails. An optical sensor measures impact velocity and a load cell measures force. The environmental chamber can be used to test materials at temperatures other than room temperature.

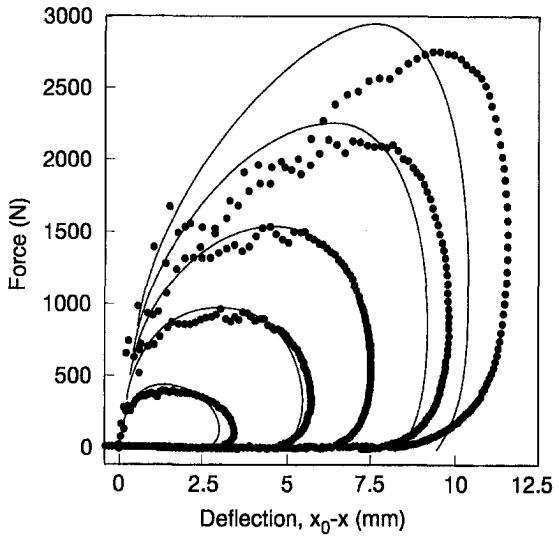

Fig. 7 Force as a function of deflection, for a sample of Wingfoot XL with an initial diameter of 24.6 mm and thickness 25.4 mm, impacted by a tup of diameter 38.1 mm and mass 1.81 kg, at 25 ± 1°C. Impact velocities are v_0 = 1.04, 2.11, 3.08, 4.11, and 4.93 m/s. In this and the following plots of impact force: (1) the symbols represent experimental data and the lines are predictions of the theoretical model, (2) increasing initial impact velocities are associated with increasing peak impact forces.

We used commercially supplied elastomeric pads for all our drop-tests. In several cases, the pads were not completely flat and the sides not completely orthogonal—i.e., the pads were slightly slanted. In instances where thinner pads were stacked together to obtain higher effective pad thickness, this lack of flatness was sometimes amplified. The crosshead rocks a little bit on the guiding rods so that the support plate and the base of the tup were usually not completely parallel at impact. The net result of all this was that at the start of the drop-test, the pad suffered a finite deformation during which its entire contact area was not *fully engaged* and the impact force rose slowly.

To account for the above experimental artifact, the computed load-deflection curves (Fig. 7 onwards)—that assume absolutely flat and parallel impacting surfaces, and instantaneous engagement of the complete contact area of the elastomeric pad—were offset to the right by a very small amount based on visual inspection of the experimental data.

3 Simulation Results

Simulation results were obtained for impacts involving flat pads and hemispherical pads.

3.1 Impact Model for Flat Surfaces. The equations for a simple uniaxial impact are given by Newton's second law, $F = m\ddot{x}$, and by relating the impact force F and the uniaxial stress σ in the material:

$$m\ddot{x}(t) = A(t)\sigma(t) \tag{6}$$

In Eq. (6), m is the mass of the tup (really of the tup and the entire crosshead assembly), $A(t)$ is the instantaneous area of impact, and $\ddot{x}(t)$ is the instantaneous acceleration of the tup. In the results presented in this paper, the area of impact of the tup is always greater than that of the pad throughout the impact. Hence, assuming volume conservation, the area $A(t)$ is inversely proportional to the instantaneous thickness of the pad; that is,

$$A(t) = \frac{A_0 x_0}{x(t)} \tag{7}$$

where A_0 and x_0 are the initial area and thickness of the pad, respectively.

The uniaxial viscoelastic stress σ_{ve} can be obtained from a model constitutive equation for an ideal Hookean incompressible viscoelastic material (Green and Tobolsky, 1946; Lodge, 1964; Treloar, 1975):

$$\sigma_{ve} = \int_{-\infty}^{t} m(t - t')[\lambda(t, t') - \lambda^{-2}(t, t')]dt' \tag{8}$$

Here $\lambda(t, t') \equiv x(t')/x(t)$ is the deformation produced during the time interval between time t' and time t. Equation (8) assumes that the deformation is a purely uniaxial one, which implies that the elastomer does not adhere strongly to the surface of the tup.

The function $m(t - t')$ contains the material's viscoelastic properties and is derived from the time-dependent linear modulus $G(t - t')$. For an incompressible rubber with a time-independent Poisson's ratio, it is given as,

$$m(t - t') \equiv \frac{dG(t - t')}{dt'} \tag{9}$$

The linear modulus $G(t - t')$, in turn, can be obtained from the G_i's and τ_i's extracted from dynamic oscillatory data for each material, as discussed in Section 2.3. Then, $G(t - t')$ is given by,

$$G(t - t') = \sum_i G_i e^{-(t-t')/\tau_i} \tag{10}$$

To the viscoelastic stress σ_{ve} is added a viscous-flow stress $\sigma_v = -3\eta\dot{x}/x$ which represents contributions from modes faster than those included in the spectrum, as discussed in Section 2.3. Hence,

$$\sigma = \sigma_{ve} - 3\eta\dot{x}/x \tag{11}$$

Here, $-\dot{x}/x$ is the rate of strain in a uniaxial compression and the factor of three enters because of Trouton's ratio (see p. 63, Larson, 1988) for volume-conserving deformations. The inclusion of the viscous-flow term leads to initial conditions on impact force given as, $F(0^-) = 0$ and $F(0^+) > 0$. This results in some of the predicted load-deflection curves, especially those corresponding to high impact velocities, to start from a force value of greater than zero (see, for instance, Fig. 7).

3.2 Comparison With Drop-Test Experiments for Flat Surfaces. Using Eqs. (6)–(11), and the viscoelastic constants from Table 2, we can now predict the forces generated during impact by solving the momentum-balance equation, as described in Larson et al. (1996), with no adjustable parameters. Figure 7 shows the measured and predicted impact force as a function of deflection for Wingfoot XL at room temperature, 25°C. Excellent agreement is obtained between measured and predicted forces, at least for the lower impact velocities, similar to the agreement found with a pad of Sorbothane 70; see Fig. 8. For the higher impact velocities, there is a slight over-prediction of peak force and a corresponding under-prediction of maximum deflection. The high hysteresis, or damping, of Wingfoot XL at room temperature is predicted very well at all impact velocities. Comparing Figs. 7 and 8 shows that the "roundedness" of the impact curves for Wingfoot XL, due to its high hysteresis, avoids the undesirable sharp force peaks observed in Sorbothane.

At an impact velocity of around 3 m/s, which is the highest impact velocity shown for Sorbothane in Fig. 8, and is an intermediate velocity for Wingfoot XL in Fig. 7, both Sorbothane and Wingfoot XL show the same maximum impact force, around 1300 N. However, for Wingfoot XL, the maximum deflection is smaller, less than 8 mm, while for Sorbothane, it is over 13 mm. The Wingfoot XL material is also capable of absorbing a more severe impact with a lower force than is Sorbothane; for an impact velocity of around 5 m/s, the peak force for Wingfoot XL is less than 2700 N, while for Sorbo-

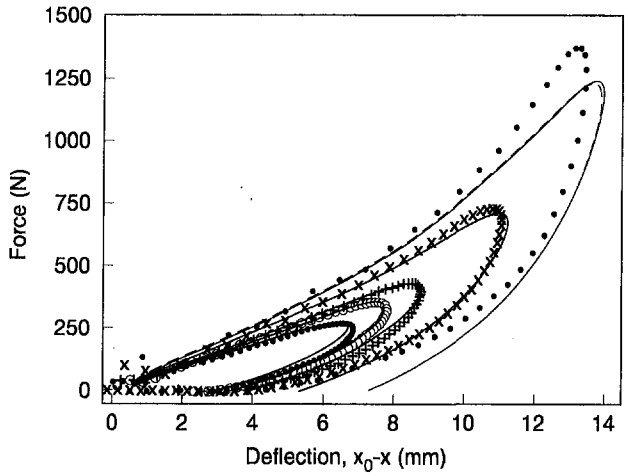

Fig. 8 Force as a function of deflection, for a sample of Sorbothane 70 with initial diameter 24.9 mm and thickness 25.4 mm, impacted by a tup of diameter 38.1 mm and mass 1.81 kg, at T = 20 ± 1°C. Impact velocities are v_0 = 1.00, 1.23, 1.44, 2.04, and 2.84 m/s. For the velocity of 2.84 m/s, there are two lines; one is for the 14-mode fit representation of the linear viscoelastic data with ν = 500 Poise, and the other is for the 15-mode representation with ν = 200 Poise. All other calculations were made with the 14-mode spectrum. (Taken from Larson et al., 1996).

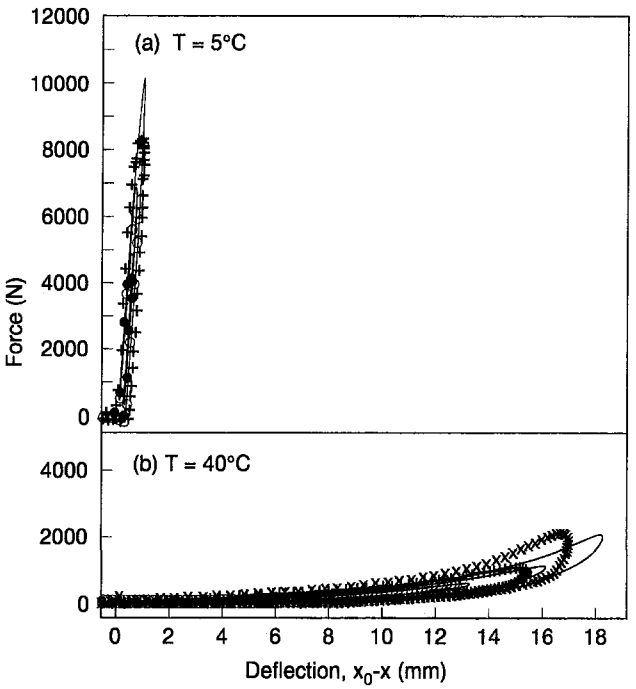

Fig. 9 Force as a function of deflection, for a sample of Wingfoot XL with initial diameter 24.6 mm and thickness of 25.4 mm, impacted by a tup of diameter 38.1 mm and mass 2.27 kg, at (*a*) T = 5 ± 1°C, and (*b*) 40 ± 1°C. The impact velocities are (*a*) v_0 = 1.04, 1.48, and 2.16 m/s, and (*b*) v_0 = 1.12, 1.66, 2.34, and 3.05 m/s.

thane, a simulation shows a peak force exceeding 3600 N. The actual peak force in Sorbothane is actually likely to be considerably larger than this, since we typically observe a growing under prediction of the peak force in Sorbothane when the deflection exceeds 40% of the pad thickness. Since the simulations predict these differences between Sorbothane and Wingfoot XL, based only on the linear viscoelastic properties of the two materials, we conclude that the linear properties exhibited by Wingfoot XL are superior, for impact-absorbing purposes, to those of Sorbothane at room temperature.

However, we noted earlier that the viscoelastic properties of Wingfoot XL are very temperature sensitive near room temperature. Figure 9 shows the impact force versus deflection for Wingfoot XL at 5°C and 40°C, respectively below and above room temperature. Note the enormous difference in impact force and deflection produced by these temperature changes. At 5°C, Wingfoot XL is a hard, glassy material that hardly deforms under an impact, and so produces a very high impact force, around 8000 N, even for an impact velocity of only around 2.1 m/s. For comparable pads of Sorbothane at an even lower temperature of −5°C, a similar impact velocity produced a peak force of less than 1600 N. Thus, Sorbothane is a much more acceptable impact-absorbing material at low temperatures than is Wingfoot XL.

At high temperatures, T = 40°C, Wingfoot XL is more acceptable, and its behavior is comparable to that of Sorbothane at 40°C. However, at elevated temperatures neither Wingfoot XL nor Sorbothane are ideal, because for an impact velocity of around 3 m/s, they deflect by over 60% of their initial thickness; hence, very high peak forces would occur if the drop velocity were to increase by even a modest amount at this temperature.

We now consider the effect of sample geometry on the impact characteristics of Wingfoot XL. Earlier, we showed for Sorbothane that there is good agreement between model predictions and experimental data when the pad diameter is in the range 25.4–38.1 mm, and for pad thicknesses of 12.7–38.1 mm. Figure 10 shows that for Wingfoot XL, agreement similar to that of Fig. 7 is also obtained with the model for a wide pad of diameter 38.1 mm. No doubt the model would also be successful in describing impacts with pad thicknesses in the range 12.7–38.1 mm for Wingfoot XL, just as was the case for Sorbothane.

It is more important to us for our application, however, to determine whether or not the model can describe impacts involving thin pads. To answer this question, we perform impact tests using 25.4 mm diameter pads of Wingfoot XL, with thicknesses in the range 12.0 mm down to 3.05 mm. Figure 11 shows that the most important gross characteristics of an impact, namely the peak force and the maximum deflection, are fairly accurately predicted by the model, even for the thinnest, 3.05 mm thick pad. Note, however, that as the pad becomes thinner, the measured force appears to become noisier; the noise is especially prominent in the 3.05 mm thick pad. The apparent noise in these thin-pad data is produced by a fairly regular oscillation in force as a function of time; see Fig. 12. The period of the oscillation is around 0.35–0.25 ms, decreasing somewhat

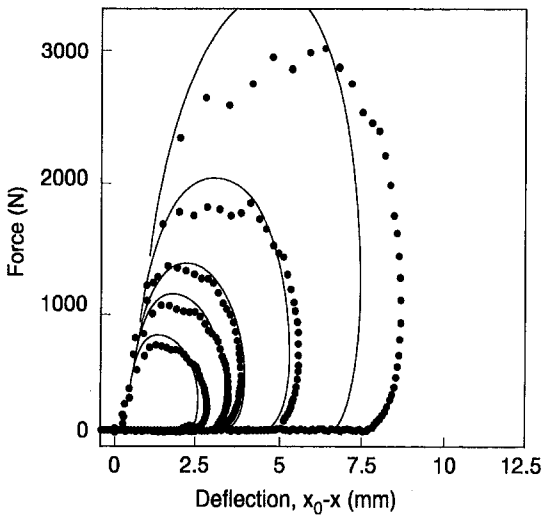

Fig. 10 Force as a function of deflection, for a sample of Wingfoot XL with initial diameter 37.3 mm and thickness 25.4 mm, impacted by a tup of diameter 50.8 mm and mass of 1.82 kg, at T = 26 ± 1°C. The impact velocities are v_0 = 1.26, 1.75, 2.11, 3.08, and 4.94 m/s.

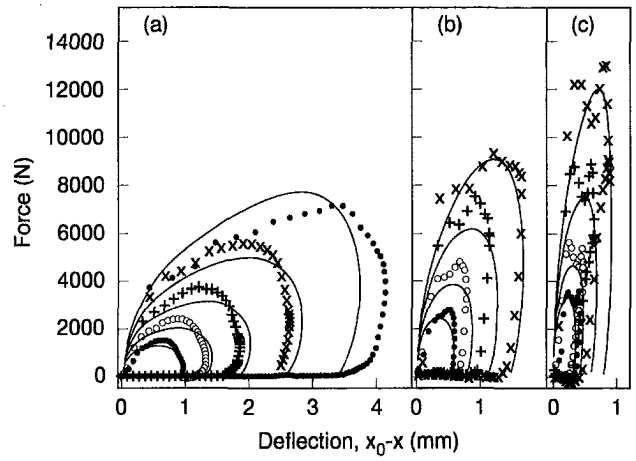

Fig. 11 Force as a function of deflection for samples of Wingfoot XL of varying thickness, impacted by a tup of diameter 38.1 mm and mass 1.81 kg. (*a*) x_0 = 12.0 mm, D_0 = 26.7 mm, T = 22 ± 1°C, and v_0 = 1.06, 1.60, 2.38, 3.51, and 4.94 m/s. (*b*) x_0 = 6.25 mm, D_0 = 27.4 mm, T = 22 ± 1°C, and v_0 = 1.10, 1.73, 2.62, and 3.62 m/s. (*c*) x_0 = 3.05 mm, D_0 = 27.4 mm, T = 23 ± 1°C, and v_0 = 1.03, 1.41, 2.12, and 3.05 m/s.

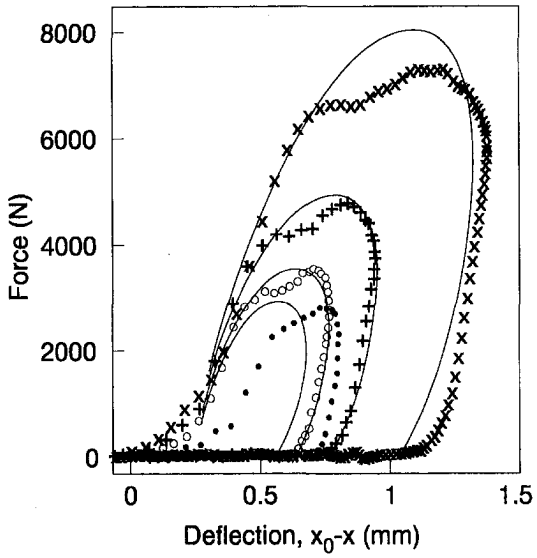

Fig. 13 Force as a function of deflection for a sample of Impactek solid with an initial diameter of 25.1 mm, and thickness of 9.86 mm, impacted by a tup of diameter 38.1 mm and mass 1.81 kg, at T = 20 ± 1°C. Impact velocities are v_0 = 1.01, 1.23, 1.69, and 2.66 m/s.

as the impact velocity increases. These oscillations are not predicted by the model.

The existence of the oscillations, and their increasing severity with decreasing pad thickness, suggest that they are caused by a viscoelastic deformation wave that is launched into the material on impact. Since the elastomer is viscoelastic, and not purely elastic, any such wave will disperse or damp out over time. For thin enough bodies, however, the time required for the wave to propagate through the pad and to be reflected back to the tup (where the force is measured) might become comparable to the time required to dissipate the wave. In such a case, an oscillation, or "ringing" of the force transducer would occur, such as that shown in Fig. 12. For an ideal elastic body, the speed of a deformation wave moving through the pad is roughly $\sqrt{G/\rho}$, where G is the elastic modulus and ρ is the material density. At the frequency of the impact, the modulus of Wingfoot XL is roughly 10^7 N/m^2, which would yield a wave speed of around 10^2 m/s, if the material were purely elastic. Propagation of a wave of this speed through a pad 3 mm thick, and reflection of that wave back to the impacting surface would therefore require around 0.06 ms, which is about three times smaller than the observed oscillation period. Of course, our material is far from being purely elastic, and an accurate estimation of the wave speed and its rate of dissipation would require a complex analysis of a nonuniform time-dependent deformation of the elastomer under the given impact conditions.

Whatever the source of the oscillation is, the important point for our purposes is that it does not greatly affect the peak force, maximum deflection, or impact duration, at least for pads no thinner than 3 mm thick. Thus, our simple analysis, which cannot predict such oscillations, can still be used to predict the important gross features of the impact, even for fairly thin pads.

Drop tests were also performed for Impactek and E.A.R. C-1002 over a range of drop heights similar to that used for Wingfoot XL. Using the constants shown in Table 2, the impact predictions for these materials are in good-to-excellent agreement with the experimental results; see Figs. 13 and 14. Note that 4 thinner pads were stacked together to obtain the pad thickness of 9.86 mm for Impactek in Fig. 13. We believe that there was some compaction of the loose stack that occured at first impact, v_0 = 1.01 m/s, that led to the wider offset we see

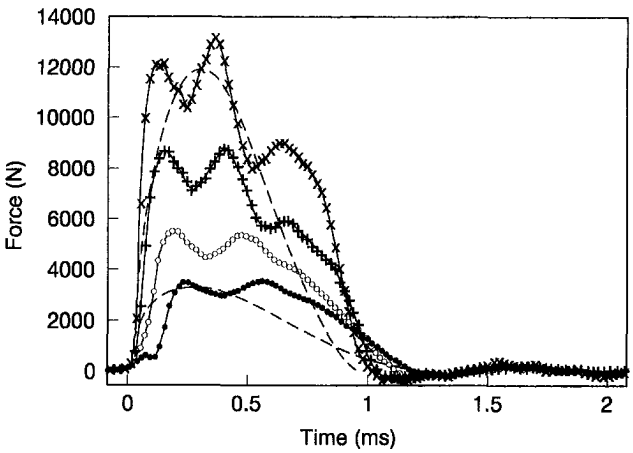

Fig. 12 The data in Fig. 11(*c*) for a 3.05 mm thick pad of Wingfoot XL are replotted as force versus time. The solid lines are guides to the eye; the dashed lines are the model predictions for the lowest and highest velocity impacts.

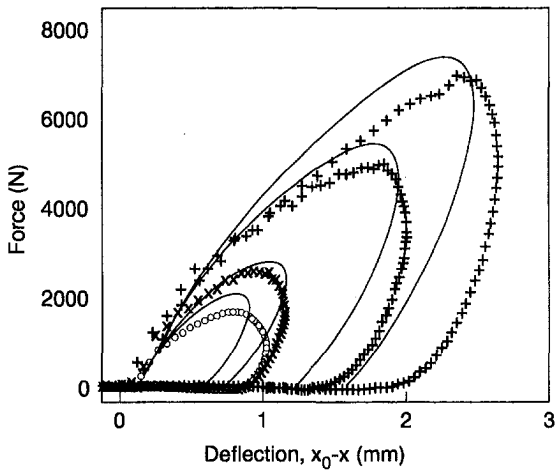

Fig. 14 Force as a function of deflection for a sample of E.A.R. C-1002 with an initial diameter of 32.4 mm, and thickness of 12.5 mm, impacted by a tup of diameter 50.8 mm and mass 1.82 kg, at T = 20 ± 1°C. Impact velocities are v_0 = 1.06, 1.41, 2.61, and 3.42 m/s.

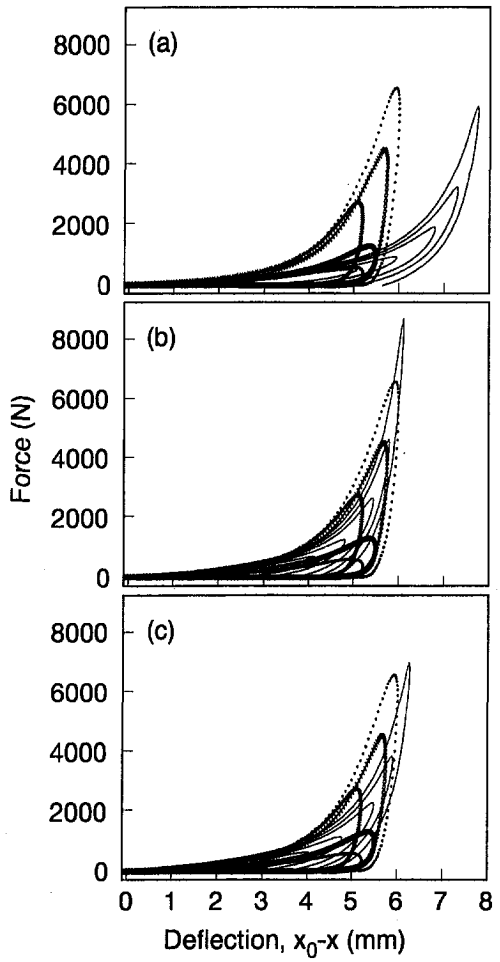

Fig. 15 Force as a function of deflection for a hemispherical sample of Sorbothane with D_0 = 18.8 mm, impacted by a tup of diameter 38.1 mm and mass 1.81 kg, at velocities of 1.10, 1.48, 2.00, 2.44, and 3.01 m/s. The lines are predictions of the theory for an "equivalent flat pad." In (a) $x_{0,\text{eff}} = D_0/2$ = 9.4 mm and $A_{0,\text{eff}} = \frac{2}{3} \times (\pi D_0^2/4)$ = 185 mm². In (b) $x_{0,\text{eff}} = \frac{2}{3} \times (D_0/2)$ = 12.5 mm and $A_{0,\text{eff}} = \pi D_0^2/4$ = 277.5 mm². In (c) $x_{0,\text{eff}} = \sqrt{\frac{2}{3}} \times (D_0/2)$ = 15.3 mm and $A_{0,\text{eff}} = \sqrt{\frac{2}{3}} \times (\pi D_0^2/4)$ = 226.5 mm².

in the experimental data for that velocity. Our model predicts the peak force and deflection for E.A.R. C-1002 fairly well (Fig. 14) although it under-predicts the hysteresis.

3.3 Model for Hemispherical Surfaces. When portable electronic devices are accidentally dropped, the impact often occurs at a corner or edge of the device. The shape of the shock-absorbing rubbery layer around a corner or edge is obviously not flat, and the deformation of the elastomer will be both nonuniform and nonuniaxial. To study the effects of these geometric nonidealities, we measured the forces during the impact of flat tups against hemispherically shaped samples of Sorbothane elastomer as shown in Fig. 1(*b*). The deformations and forces involved in such an impact might mimic those that occur when the elastomer-protected corner of an electronic devices impacts a flat surface. Figure 15(*a*) shows the force as a function of deflection for a hemispherical sample of Sorbothane with an initial diameter D_0 = 18.8 mm impacted by a tup of diameter 38.1 mm and mass 1.81 kg, at various impact velocities. The force is very low at first, but then rises very steeply. Accurate modeling of such an impact is difficult, since it requires accounting for the nonuniaxial, nonuniform character of such an impact. Presumably an axisymmetric finite element analysis could accurately predict the deformation and the forces, but for a viscoelastic material this would be very time consuming—both to develop the computer code and to run it.

We therefore seek a "quick analysis" with which we hope to make qualitative, if not quantitative, predictions. In developing such an analysis, we seek to use the tool at hand, namely the model for uniform uniaxial impacts. The simplest computational approach is to replace in the analysis the hemispheric shape with an "effective flat pad" whose area and thickness are chosen judiciously to represent the relevant dimensions of the hemisphere. If we insist that the volume V of the effective pad be the same as that of the hemispherical sample that it replaces, the product of the initial area $A_{0,\text{eff}}$ and thickness $x_{0,\text{eff}}$ of the effective pad must equal the volume of hemisphere, that is,

$$V = A_{0,\text{eff}} x_{0,\text{eff}} = \tfrac{2}{3}(\tfrac{1}{4}\pi D_0^2)(\tfrac{1}{2}D_0) = \tfrac{2}{3}A_0 x_0 \qquad (12)$$

Here $A_0 = \pi D_0^2/4$ is the cross-sectional area of the base of the hemisphere and $x_0 = D_0/2$ is its height.

Equation (12) suggests two simple ways of choosing the dimensions of the effective pad in such a way that its volume equals that of the hemisphere; namely, choose (a) $x_{0,\text{eff}} = D_0/2$ and $A_{0,\text{eff}} = \frac{2}{3} \times (\pi D_0^2/4)$, or, (b) $x_{0,\text{eff}} = \frac{2}{3} \times (D_0/2)$ and $A_{0,\text{eff}} = \pi D_0^2/4$. Combinations of these two extremes are also possible; for example, choose (c) $x_{0,\text{eff}} = \sqrt{\frac{2}{3}} \times (D_0/2)$ and $A_{0,\text{eff}} = \sqrt{\frac{2}{3}} \times (\pi D_0^2/4)$. The lines on Fig. 15 are the predictions of the quick analysis using these three sets of choices, respectively. The first choice, Fig. 15(*a*), predicts the peak forces quite accurately, but predicts maximum deflections that are too large, while the second choice, Fig. 15(*b*), accurately predicts the maximum deflections but over predicts the peak forces for high-velocity impacts. The third choice, Fig. 15(*c*), predicts a compromise—for both forces and deflections—between the above two extremes.

Figure 16(*a*) and 16(*b*) show the force as a function of deflection for a larger hemispherical sample of Sorbothane (D_0 = 31.2 mm) for "effective pad dimensions choices" (*a*) and (*b*), respectively. Observe that for the larger hemisphere, the peak force predicted when the effective area is taken to be equal to the area of the base of the hemisphere is smaller than the measured force (Fig. 16(*b*)), while for the smaller hemisphere, the predicted force under this assumption is larger than the measured force (Fig. 15(*b*)). Based on these results it seems that the choice of the most appropriate equivalent flat-pad dimensions depend, to an extent, on the hemispherical sample size.

Presumably, this indicates a dependence on the impact energy density $U \equiv Wh/V = Wh/A_{0,\text{eff}}x_{0,\text{eff}}$ and the initial strain rate $v_0/x_{0,\text{eff}}$, where W and h are the weight of the tup and its drop height, and $v_0 = \sqrt{2gh}$ is the impact velocity. Both U and the initial strain rate can be nondimensionalized. Determining the exact dependence of the "equivalent flat pad dimensioning scheme" on these nondimensional groups is beyond the scope of the current paper.

The impact energy density, and to some extent the strain rate, play an important role in determining the efficacy of commercial elastomers for shock-protection purposes, as explained below.

4 Cushioning Efficiency—"*J* Curves"

To facilitate material selection, and the design of rubbery components, suppliers of impact-absorbing materials frequently summarize impact performance data in the form of a single, so called, "*J* curve." The *J* curve is a plot of dimensionless peak force $J = F_{\max}x_0/Wh$, against impact energy density $U = Wh/x_0A_0$, where $F_{\max}$ is the maximum force generated during impact.[9] An ideal impact-absorbing material, that generates the

[9] The *J* curve is determined experimentally for an arbitrary set of drop conditions (that vary by supplier) at room temperature.

lowest peak force for given impact conditions, is one that produces constant force with deformation and allows its entire thickness x_0 to be used as "stopping distance," that is, the pad can be squeezed to zero thickness. The minimum impact force thus produced can be shown to equal Wh/x_0. Hence, the value of J corresponds to the actual peak force relative to the lowest possible peak force. Since no impact absorbing material can behave in the theoretically ideal way described above, J values always exceed unity.

The motivation for plotting J versus U comes from a dimensional analysis originally described by Woolam (1968); the equations of motion (6)–(7) can be rewritten as,

$$2\left(\frac{x_0}{v_0}\right)^2 \ddot{X} = \frac{1}{U}\frac{1}{X}\sigma(X(t)) \tag{13}$$

where $X \equiv x/x_0$ is the dimensionless instantaneous pad thickness, which is related to the instantaneous strain by $\lambda = 1/X$. Equation (13) implies that $X(t)$, and hence peak force, depend on U and v_0/x_0.

For purely elastic materials (no strain-rate dependence), the peak force would be a function of U only and values of J for a single material under varying drop conditions—weight, height, and thickness and area of pad—will fall on a single curve. For time-dependent (i.e., viscoelastic) materials, however, the J curve will depend both on U and v_0/x_0. Figure 17, for example, shows the J curves calculated using our impact theory for Wingfoot XL under conditions in which the drop mass is varied at fixed impact velocity (that is, only U is changing), and under conditions in which the impact velocity is varied

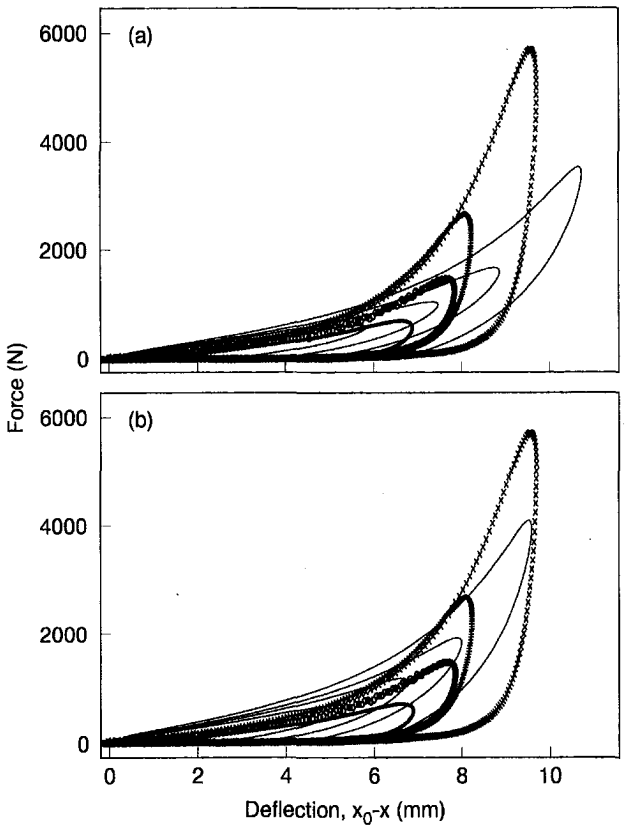

Fig. 16 Force as a function of deflection for a hemispherical sample of Sorbothane with D_0 = 31.2 mm, impacted by a tup of diameter 50.8 mm and mass 1.82 kg, at velocities of 1.02, 1.43, 2.02, 2.63, and 3.76 m/s. The lines are predictions of the theory for an equivalent flat pad. In (*a*) $x_{0,eff} = D_0/2$ = 15.6 mm and $A_{0,eff} = \frac{2}{3} \times (\pi D_0^2/4)$ = 511 mm². In (*b*) $x_{0,eff} = \frac{2}{3} \times (D_0/2)$ = 10.4 mm and $A_{0,eff} = \pi D_0^2/4$ = 766.6 mm².

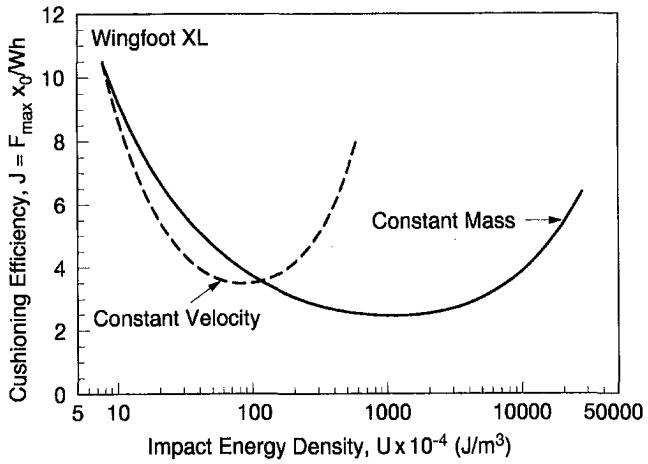

Fig. 17 Cushioning efficiency "*J*" curves calculated for a pad of diameter 24.6 mm and height 25.4 mm of Wingfoot XL. The constant mass curve is for an impacting mass of 1.81 kg and the constant velocity curve is for an impact velocity of 1.04 m/s.

and the mass kept fixed (so both U and v_0/x_0 are changing). In both cases, the thickness and area of the pad are held fixed. Note that substantially different curves are obtained in the two cases; their J minima are spaced more than an order of magnitude apart on the U-axis. (The two curves intersect at the point where the mass and velocity are identical on the two curves.) A whole family of J curves of the type shown in Fig. 17 can be generated for Wingfoot XL by varying drop velocity at each of a series of masses, or, conversely, by varying drop mass at a series of drop velocities.

Despite the dependence of the J curve on drop conditions, its usefulness as an engineering tool stems from the existence of a minimum in the J curve, suggesting the existence of a "maximum cushioning efficiency." The location of the minimum along the U-axis characterizes the drop conditions for which the material is especially well suited for optimal use of its cushioning ability. That is, for a given pad size, there exist impact conditions—and hence, an impact energy density—for which U is large enough to utilize a significant portion of the available effective stopping distance in the pad but not so large that it generates high forces. Conversely for a given U, one can select a material that has its optimum J at that U. For example, for large U, that is, heavy masses, high impact velocities, or thin, small, pads, one would like a material for which the minimum is located at a large value of U. This would correspond to a rather stiff (high modulus) material, such as Wingfoot XL.

Given the wide separation in "fixed-velocity" and "fixed-mass" J curves for Wingfoot XL, as shown in Fig. 17, it may be prudent to use the fixed mass J curve for designing elastomeric parts for a given portable product. This is because the effective mass of the product (Goyal et al., 1994) in accidental drops will vary much less than the impact velocity, which depends on the height from which the object is dropped. The minimum value of J for Wingfoot XL is around 2.4, while for Sorbothane 70, the minimum J value is predicted to be around 4.2 (Larson et al., 1996).

One of the issues that the current format for J curves does not address implicitly is their dependence on temperature. In a future publication, we shall present nondimensional groups that capture the temperature dependence of the material.

5 Conclusions and Future Directions

We have shown that a simple uniaxial impact model for elastomers, proposed by Larson et al. (1996), predicts forces and deflections as well for Wingfoot XL, Impactek, and E.A.R. C-1002, as it does for Sorbothane 70 in drop tests using flat pads

and flat impact surfaces. This shows that the linear viscoelastic spectrum in general adequately characterizes the impact properties of such commercially available rubbery materials that are recommended for use in shock-protection of products. In addition, comparisons of the impact properties of these materials can now be made, and the differences between them can be traced to differences in their relaxation spectra—a fundamental and engineerable property. At room temperature, for example, Wingfoot XL is more dissipative than Sorbothane, and is a more nearly ideal impact absorber, but these properties degrade quickly at lower temperature, due to the high temperature sensitivity of the viscoelastic relaxation spectrum of this material.

We have also shown that the important characteristics of the impact, namely its maximum force, pad deflection, and impact duration, can be predicted even for pads of Wingfoot XL as thin as 3 mm thick, even though oscillations present in the thin-pad data (probably due to viscoelastic-wave propagation) are not predicted. The ability to predict impact forces in very thin pads is important in light-weight designs for portable electronic products, in which the mass and size of elastomer used for shock-protection is reduced to a bare minimum.

In addition, qualitative predictions can be made for nonideal shapes, such as hemispheres, by replacing, for calculation purposes, the hemispherical shape by an effective flat pad whose volume is the same as that of the hemisphere, but whose cross sectional area or height (or both) are somewhat smaller than that of the hemispherical sample.

The next steps in our research program are to predict impact forces for foamed materials, which are popular for impact protection, and to develop general material design principles that allow choice of the optimal material—one that minimizes the peak impact force—for a given set of impact conditions including temperature. Beyond these immediate steps, two longer term projects can be envisioned.

Using finite element (FEM) simulations, the effect of hemispherical and other shapes can be simulated rigorously by accounting for the nonuniformity of the deformation. The results from this FEM study can be reduced to general product design guidelines. Secondly, these simulation techniques can be incorporated into 'whole-product' simulators in which deflections and forces in the shock-absorbing rubber are coupled to the mechanical response of other parts of the product. With these additional steps, we hope by computer simulation to be able to predict in detail impact forces that occur during accidental drops of portable electronic devices, and to provide a new design tool for improving their ruggedness.

Acknowledgments

We would like to acknowledge the help of Leo Penn and Claire Plagianis with the rheological measurements. We wish to thank Ernie Lauber from Sorbothane Inc.; Vic Pilkington from the Goodyear Tire & Rubber Company; Mike Blanner, Alan Seville and Jim Palombo from E.A.R. Specialty Composites; and John Clayman from Frelonic Corporation for supplying us with material samples for our experiments. We would also like to thank Rich Howard, Paul Mankiewich, Lou Manzione, and Paul Sullivan for support.

References

Burnett, D. S., 1987, *Finite Element Analysis: From Concepts to Applications,* Addison-Wesley Publishing Company, Reading, MA.

Chen, C. P., and Lakes, R. S., 1990, "Design of Viscoelastic Impact Absorbers: Optimal Material Properties," *International Journal of Solids and Structures,* Vol. 26, pp. 1313–1328.

E.A.R. Speciality Composites, 1996, Technical Data Sheet TDS-19, Indianapolis, IN.

Ferry, J. D., 1980, *Viscoelastic Properties of Polymers,* Third Edition, Wiley, New York.

Goyal, S., Pinson, E. N., and Sinden, F. W., 1994, "Simulation of Dynamics of Interacting Rigid Bodies Including Friction II: Software System Design and Implementation," *Engineering With Computers,* Vol. 10(3), pp. 175–195.

Goyal, S., Papadopoulos, J., and Sullivan, P., 1997, "Shock Protection of Portable Electronic Products: Shock Response Spectrum, Damage Boundary Approach, and Beyond," *Shock and Vibration,* Vol. 4(3), pp. 169–191.

Goyal, S., Papadopoulos, J., and Sullivan, P., 1998a, "The Dynamics of Clattering I: Equation of Motion and Examples," ASME *Journal of Dynamic Systems, Measurement, and Control,* Vol. 120(1), pp. 83–93.

Goyal, S., Papadopoulos, J., and Sullivan, P., 1998b, "The Dynamics of Clattering II: Global Results and Shock Protection," ASME *Journal of Dynamic Systems, Measurement, and Control,* Vol. 120(1), pp. 94–102.

Goyal, S., Upasani, S., and Patel, D., 1998c, "Designing Best-In-Class Impact-Tolerant Cellular Phones & Other Portable Products," *Bell Labs Technical Journal,* Vol. 3(3), pp. 159–174.

Green, M. S., and Tobolsky, A. V., 1946, "A New Approach to the Theory of Relaxing Polymeric Media," *Journal of Chemical Physics,* Vol. 14, pp. 80–92.

Larson, R. G., 1988, *Constitutive Equations for Polymer Melts and Solutions,* Butterworths, Boston.

Larson, R. G., Goyal, S., and Aloisio, C. J., 1996, "A Predictive Model for Impact Response of Viscoelastic Polymer in Drop Tests," *Rheologica Acta,* Vol. 35, pp. 252–264.

Lodge, A. S., 1968, "Constitutive Equations from Molecular Network Theories for Polymer Solutions," *Rheologica Acta,* Vol. 7, pp. 379–392.

Macosko, C. W., 1994, *Rheology Principles, Measurements, and Applications,* VCH Publishers, New York.

Pilkington, M., Creasey, J., and Becken, R., 1985, "Energy Absorbing Rubber Composition," United States Patent Number 4504604, March 12.

Pilkington, M., 1995, Personal Communication, Goodyear Tire Company, Akron, OH, May 15.

Rosen, S. L., 1993, *Fundamental Principles of Polymeric Materials,* Second Edition, Wiley, New York.

Seville, A., 1998, Personal Communication, E.A.R. Speciality Composites, Indianapolis, IN, July 10.

Treloar, L. R. G., 1975, *The Physics of Rubber Elasticity,* Third Edition, Clarendon Press, Oxford, UK.

Woolam, W. E., 1968, "A Study of the Dynamics of Low Energy Cushioning Materials Using Scale Models," *J. Cellular Plastics,* Vol. 4, pp. 79–83.